Journal of Mines, Metals and Fuels, *71(11): 2202-2211; 2023. DOI: 10.18311/jmmf/2023/36040*

Print ISSN : 0022-2755

Journal of Mines, Metals and Fuels

Contents available at: *www.informaticsjournals.com/index.php/jmmf*

Hydrodynamic Analysis of NACA 4415 Hydrofoil for Marine Applications

Md. Ayaz. J. Khan[1]*, Sanjay D. Pohekar[2], Pramodkumar M. Bagade[3]

[1]Assistant Professor, Tolani Maritime Institute, Pune - 410507, Maharashtra, India; mdayazjkahn@gmail.com
[2]Symbiosis International (Deemed) University, Pune - 412115, Maharashtra, India; head_resprog@siu.edu.in
[3]Bhivarabai Sawant College of Engineering and Research, Pune - 411041, Maharashtra, India; pramodbagade@gmail.com

Abstract

In the present research, Computational Fluid Dynamics (CFD) analysis has been conducted to investigate the practical utility of ducted design for marine propellers for a range of Reynolds numbers (Re). Hydrodynamic characteristics are investigated for ducted propeller –Kort nozzle for various duct angles ($0^o \le \alpha \le 10^o$). The Kort nozzle duct section is less explored with NACA hydrofoils and has been a hot research topic in the domain. Here, the hydrodynamic characteristics of the duct section are numerically investigated, considering NACA4415 foil. All the simulations are performed using ANSYS-FLUENT in a range of $1\times10^6 < Re < 5\times10^6$. We have used the k –ω SST turbulence model during our investigation. The performance of NACA4415 is evaluated concerning the lift, drag, and pressure coefficient for various angles of attack ($-12^o < \alpha < 12^o$). These models were employed for nozzle configuration at different shroud/duct angles ($0^\circ < \alpha_d < 10^\circ$). It is found that the ducted configuration for the considered hydrofoil performs the best with a duct angle $4^o < \alpha_d < 6^o$ with respect to hydrodynamic characteristics.

Keywords: *CFD, Flow Separation, Hydrofoil, Kort-Nozzle, Marine Application, NACA4415*

1.0 Introduction

The concept of ducted[1] profile was initially adopted for aircraft applications, followed by its marine application *via* Kort nozzle. One of the mostly adopted definition of Kort nozzle is "a cylindrical fitting around a propeller, tapered in-ward toward the stern to increase thrust and manoeuvrability". It is essentially constructed in a shroud form encircling a ship's propeller. It was created using hydrodynamic principles. The shroud opening is largest at the inlet, narrowest at the centre (where the propeller turns), and smallest at the outlet or exit. The major goal of this setup is to avoid separation in the wake zone and deliver increased flow close to the propeller.

Kort nozzles are more efficient than bare propellers[1–3], producing 50% greater thrust per unit power than a propeller without a duct. These nozzles, which lose their advantage over bare propellers at about 10 knots (18.5 km/h), can be improved if the shroud is shaped like a foil. The Marine Research Institute, Netherlands (MARIN) developed different nozzle designs for unique thrust characteristics, e.g., MARIN Nozzle No. 19A, 37, 22, and 24. However, the NACA airfoil sections for duct design are less explored. The present work, the NACA4415 is analyzed for the Kort-nozzle duct section using computational fluid dynamic analysis. The study addresses the performance of NACA4415 as a hydrofoil and explores the dynamics of fluid flow separation, pressure, velocity distribution, and lift and drag forces acting on the shroud. During towing and trawling conditions, particularly at low speeds, the ducts were found to provide 50% of the total power.

**Author for correspondence*

For such situations, Kort nozzles were used producing larger thrust at low speeds. For a Kort nozzle, the thrust is calculated as

$$T = T_p + T_n \quad (1)$$

where, T_p = the propeller thrust and T_n =the duct thrust.

According to commercial practice, majority of the ducted propellers employ accelerating ducts[4]. The theoretical approach to ducted propeller functioning was expanded by Tsakonas and Jacobs[5] explored the theoretical approach for investigation of propeller performance in the presence of wake, which was formed due to interaction of fluid and the propeller surface.

1.1 Flow Separation and its Control

It has been well established that the flow separation reduces the effective lift (also increases drag), so it is imperative to investigate the flow separation. During hydrodynamic analysis by[6], it was noted that stall should be at least delayed, if not at all possible to avoid it. Such delay in stall results in improved performance during turning of the ships. By lessening the size of the pressure difference over the body, streamlining decreases drag[7]. Due to decreased pressure gradient, the fluid flows without separation till the trailing edge leading to better hydrodynamic performance. During separation, a wake is generated downstream. The wake left by the body is thin because there is little flow distortion and barely any pressure drag. Due to flow instability, the boundary layer separates too soon. Compared to "turbulent flow," a "laminar boundary layer" is more prone to early flow separation. The authors also pinpointed the separation site and implemented strategies to postpone separation.

The wall-bounded flow separates when specific constant or irregular flow characteristics are present. The boundary layer will keep growing as long as there is no pressure difference along the hard surface. For a negative pressure, the boundary layer's thickness dramatically increases. Pressure and shear effects are detrimental as a result of the momentum loss. If any of them are successful for a substantial surface length, a process known as flow separation occurs that prevents the creation of the boundary layer[8].

The separation criterion is defined as in the close vicinity of the wall[9]. The wall shear stress, $\tau w = 0$ at the separation point. The adverse pressure is still present, and downstream from this point, the flow acts in the other direction, causing a backflow[10]. Increased energy losses, instability, and a postponed detachment process are all effects of flow separation. Form drag (caused by pressure differential) and skin friction drag (caused by shear stress on the wall) make up the final (net) drag force exerted on the body. Regarding basic flow physics and practical applications, literature has placed a lot of focus on separation control. Therefore, the purpose of the current study's investigation of separation is described in the sections that follow.

2.0 Background and Literature Review

Numerous efforts are being undertaken to increase the propulsive efficiency of ship and in recent years, it has received a special attention. However, detailed researches on the flow separation control over hydrofoils are very limited both experimentally and computationally. Taketani *et al.*[11] reported a parametric study on designing of a modified Kort-nozzle propeller, which demonstrated better bollard pull performance. Caldas *et al.*[12]. The RANSE model was used to numerically explore different shapes of controllable pitch propellers. A ferryboat's duct geometries were examined by Celik *et al.*[13] in order to determine the best option in terms of hydrodynamic performance. The authors assessed the performance of various duct sections and the ideal duct design for the Kort-nozzle propeller. Yu *et al.*[14] reported propeller performance under open-water conditions. Krzysztof *et al.*[15] emphasized the importance of duct shape on the thrust of ducted propellers. Xueming *et al.*'s[16] investigation of the ducted propeller's hydrodynamic performance while contrasting several turbulence models. The pressure distribution on the propellers' surfaces was examined by the authors. The velocity and pressure field around the ducted propeller was also studied. The authors show that the Reynolds Stress Model (RSM) performs better than conventional turbulence models. Similar research was done on the Kort-nozzle by Chamanara *et al.*[17]. By using ducted propellers working in oblique flow, Majdfar *et al.* conducted numerical investigations[19–21]. The comparison of accelerating and decelerating ducted propellers was published by Razaghian *et al.*[18]. They looked into how the ducted propeller's length and pitch affected hydrodynamics. In this research, the post-processing

stage of CFD analysis is expanded upon using wall shear and velocity vector plots to identify flow separated at the NACA4415 hydrofoil surface. Recent studies have focused on certain aspects of turbulent flow control related to reducing drag[22] and postponing flow separation on wings and bodies.

To lessen the drag force in flow over an airfoil, numerous studies have been carried out. This can be done by maintaining a thin boundary layer, which in turn can be done by limiting pressure loss at the trailing edge. An investigation of 2D subsonic flow over a NACA0012 at a Re range of 3106 was published by Douvi C. Eleni *et al.*[23]. Different turbulence models were used for this under steady-state circumstances. The investigation of several turbulence models and additional research on separation location identification were highlighted by the authors. Avi Seifert *et al.*[24] investigated a shock-wave boundary-layer interaction-related flow separation delay for the NACA0012 and NACA0015 airfoils under severe compressible and incompressible flow conditions.

Sudarsono *et al.*[25] tested the aerodynamic performance of a modified NACA4415 airfoil at varied free stream velocities and angles of attack. They found that the modified NACA4415 airfoil has a higher lift and momentum coefficient. Oukassou *et al.*[26] used three models—Spalart-Allmaras, k-(RNG), and k-shear stress transport—to compare the power, lift, and drag of the NACA0012 and NACA2412 airfoils (SST). Xu *et al.*[27] employed two models of steady Reynolds-Averaged Navier-Stokes (RANS) and unsteady Reynolds-Averaged Navier-Stokes to simulate the S809 (URANS) airfoil. RANS and hybrid large-eddy simulations of turbulent flow past an Aerospatiale A-Airfoil approaching stall at Re = 2.1 x10^6, M = 0.15, and = 13.3 as well as a NACA0012 airfoil under static stall circumstances at Re = 2.1x10^6, M = 0.15 at Re = 1.0×10^6, M = 0.1, α = 16.7 ∘ ., were performed by Jianghua Ke *et al.*[28].

Several studies have been undertaken to understand the aerodynamic behavior of symmetric and cambered airfoils. C.A. Baxevanou *et al.*[29] compared various turbulence models and numerical schemes for its accuracy and computational cost. One of the aims during this study was to predict transient flow at fixed points around cambered airfoils. Sarraf C. *et al.*[30] experimentally investigated the hydrodynamic behavior of 2–D NACA (15%, 25%, and 35%) symmetric hydrofoils at Re = 5×10^5. The authors provided insight on hysteretic behavior at the static stall angle, and boundary layer structures for thick hydrofoils. Dwayne A. *et al.*[31] observed that Re variations in the time-averaged flow over the foil to investigate flow separation for critical Res.

The effect of the shroud on the performance has been experimentally investigated by[32]. The authors reported that a higher power could be generated with shrouds. Power enhancement was found to be 91%, 87%, and 75% for divergent-ducted shroud in the same flow velocities. The propulsor efficiencies for ducted propellers are more significant than non-ducted ones[33]. Turbines operating inside a duct are found to enhance the power output of similarly sized rotor devices deployed in relatively low-energy currents[34]. These studies suggest that the ducted propellers can be effectively used for improved performance. However, a detailed research is needed to find the crucial factors in deciding the parameters. The present study aims at investigating such important parameters and is reported as follows.

3.0 Governing Equations, Boundary Conditions and Methodology

In order to investigate the dynamics of fluid flow separation, pressure, velocity contour, and lift and drag coefficients, the hydrodynamic performance of the NACA4415 is examined at various angles of attack. The computations are carried out using ANSYS. Fine grids are employed for all the computed presented here, considering the grid metrics like orthogonality. The importance of orthogonality and other grid metrics have been reported by Bagade *et al.*[35]. To simulate a flow over NACA4415 airfoil at a different angle of attacks ($-12^\circ < \alpha < 12^\circ$). Both steady state and transient analysis are performed.

3.1 Governing Equations

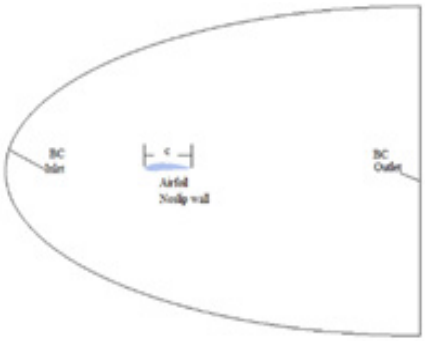
The governing equations of fluid flow are mass and momentum conservations as given by Equations (2) and (3). The *Re* considered for the present simulation are in a subsonic region and simulations are conducted in *2D* domain.

$$\frac{\partial \rho}{\partial t} + \nabla \bullet \rho \vec{V} = 0 \qquad (2)$$

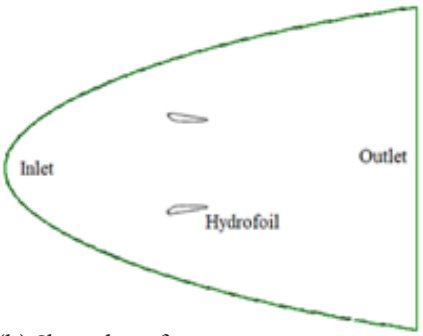
$$\frac{\partial V}{\partial t}+\vec{V}\bullet\nabla\vec{V}=-\frac{1}{\rho}\nabla(\vec{p}+\rho gz)+\upsilon\nabla^2\vec{V} \quad (3)$$

3.2 Geometry, Foil Section and Fluid Domain

The inlet (upstream) and outlet (downstream) boundaries were taken as 15 and 30 times the chord length, respectively.



(a) Computational domain for a single hydrofoil.



(b) Shroud configuration.

Figure 1. Schematic of the computational domain for different configuration.

Figure 1 shows the computational domain used for the present investigation for a single hydrofoil (Figure 1(a)) and shroud configurationn (Figure 1(b)), while Figure 2 shows a zoomed view of the hydrofoil. A nearly orthogonal grid (Figure 3) is generated for the present numerical investigation following the importance of grid metrics[35]. Figure 4 shows the wall resolution details. A fine grid is generated using 898804 elements. y+ at the airfoil surfaces is $y+_{min}$ =0.0566 and $y+_{max}$ =1.157, respectively, whereas the minimum cell wall distance is 0.0129 mm and the maximum wall distance is 0.0154. Viscous-Turbulent: k–ω SST is employed for the present computation since it provides an acceptable level of accuracy in open water conditions and unsteady flow predictions[36].

3.3 Boundary Conditions

The following boundary conditions are applied during simulations. Figure 5(a) and 5(b) show a zoomed view of the grid near the leading and trailing edge of the hydrofoil. It can be seen that a very fine grid (~10^{-5}) is used near the hydrofoil surface, while an orthogonal grid is used in the vicinity of the hydrofoil. The importance of grid metrics and orthogonal grid generation[35] is preferred.

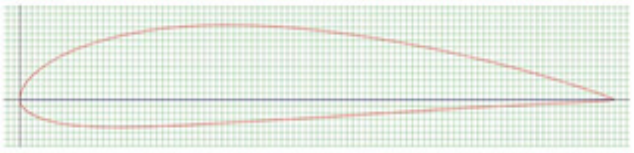


Figure 2. Zoomed view of the hydrofoil.

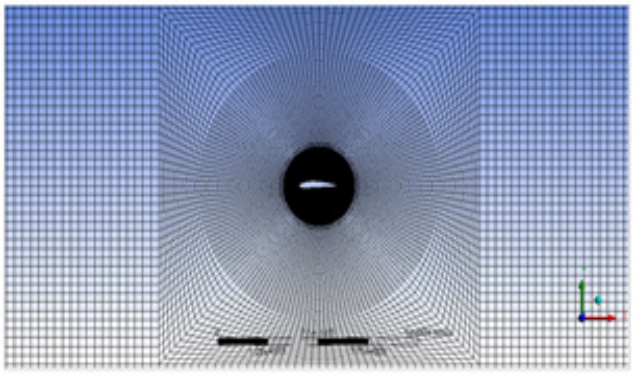


Figure 3. A nearly orthogonal grid generated around the hydrofoil.

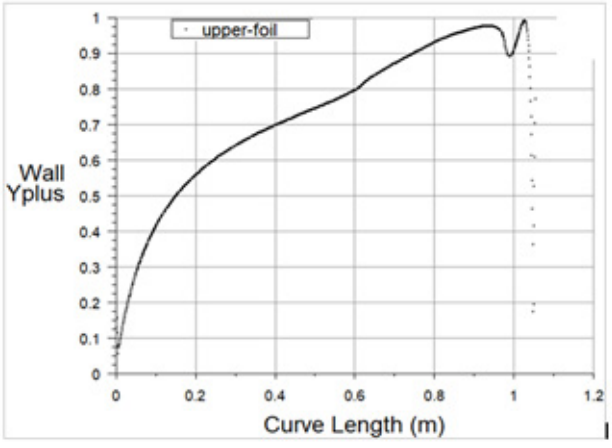
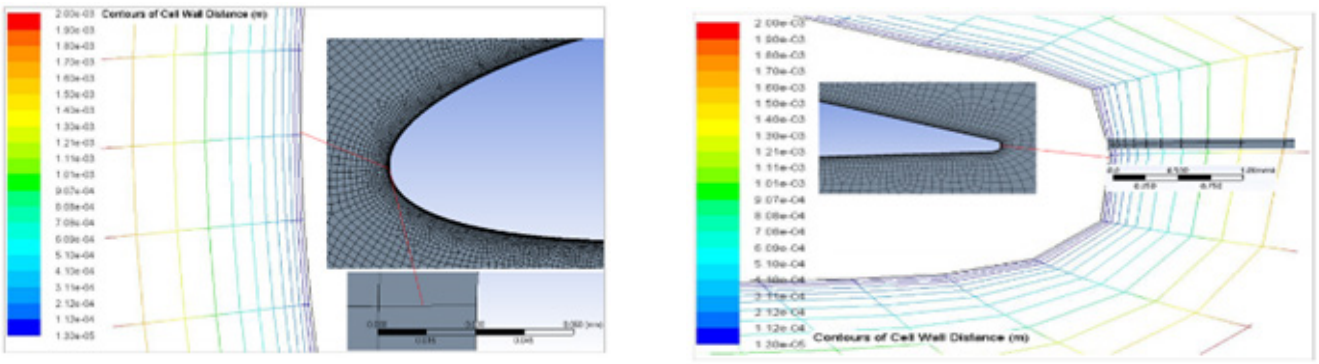


Figure 4. Grid resolution near the hydrofoil surface. ($y+_{min}$ = 0.0566 and $y+_{max}$ = 1.157).



(a) Zoomed view near the lead-ing edge of the hydrofoil. (b) Zoomed view of grid near the trailing edge of the hydro-foil

Figure 5. Details of grid around hydrofoil. A nearly orthogonal grid generated with a wall resolution $\sim 10^{-5}$.

4.0 Results

Before investigating the effects of the shroud, flow past a single hydrofoil is studied for validation purpose. Upon receiving a good match with the established results, effects of shroud (ducted profile) is further investigated for different configuration. In the following, we present results of a single hydrofoil analysis, followed by shroud configuration.

4.1 Investigation of Hydrodynamic Performance of a Single Hydrofoil

The NACA4415 hydrofoil is analyzed for a range of angles of attack ($-12^\circ < \alpha < 12^\circ$). Figure 6 and 7 show the pressure coefficient Cp and pressure distribution contours

Table 1. Boundary conditions applied during simulations

Inlet:	Velocity-inlet
Outlet:	Pressure-outlet
Models and Materials:	Fluid-Water
Viscosity of fluid	$0.001 Pa-s$
Models:	Viscous-Turbulent: $k-\omega$ SST
Density of fluid	$1000 kg/m^3$
Problem Setup:	Pressure Based
Reynolds Number	1×10^6 (varies from case to case)

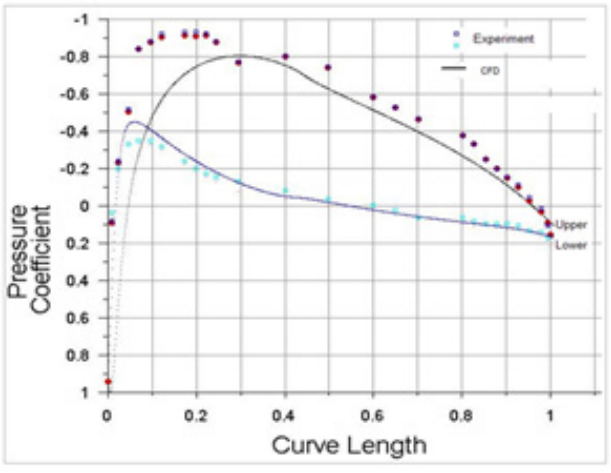


Figure 6. Pressure coefficient *Cp* at $\alpha = 0.15^\circ$.

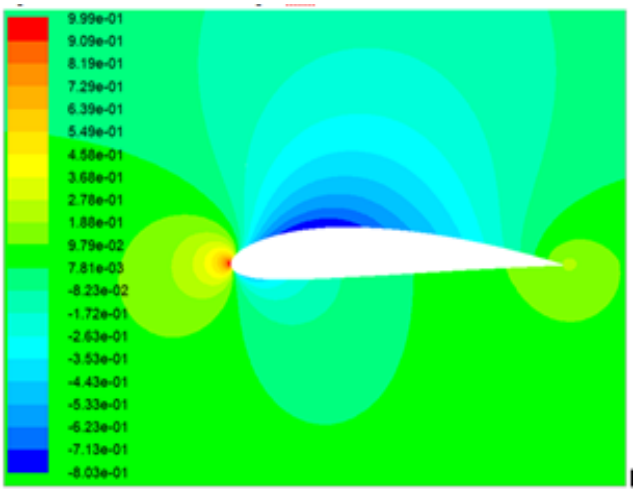
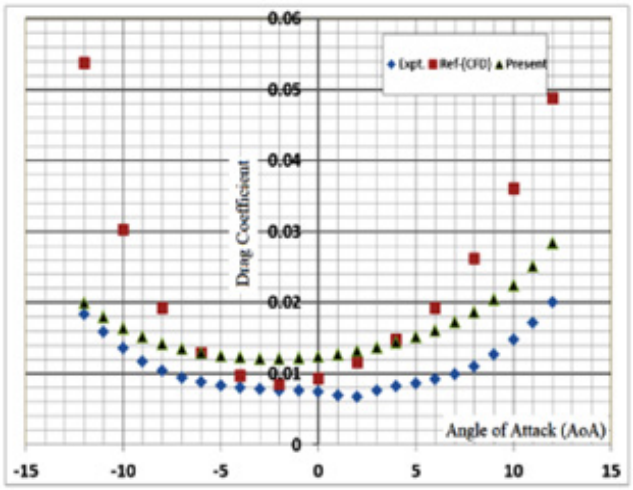
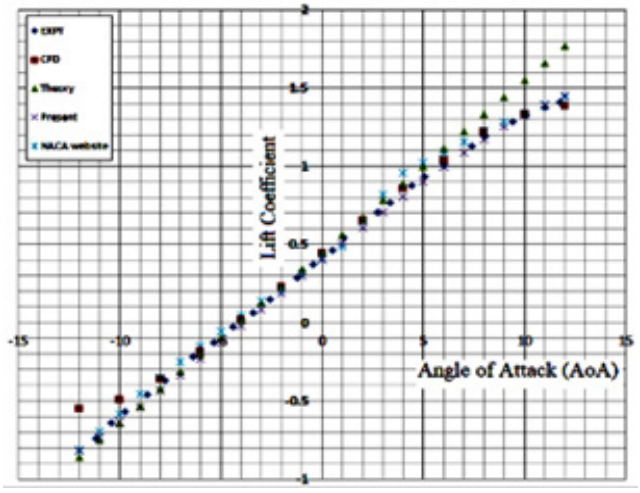


Figure 7. Pressure contours at $\alpha = 0.15^\circ$.

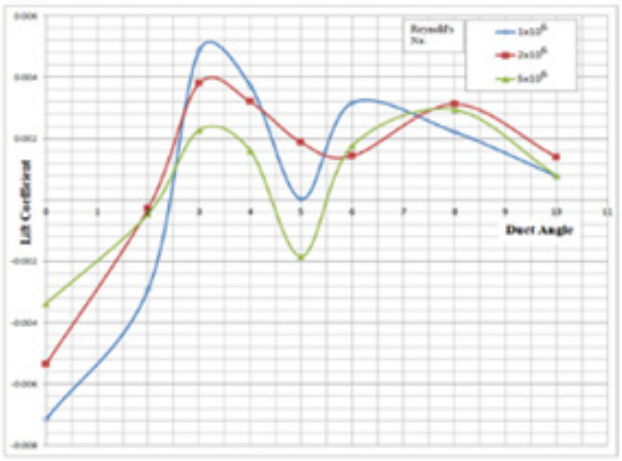


(a) Drag coefficient, (c_d) at different angles of attack, α

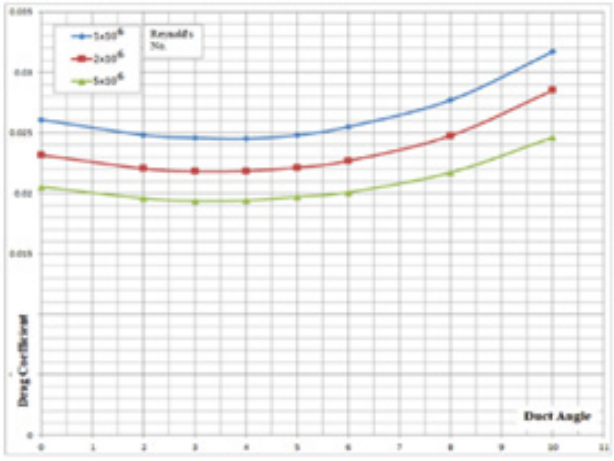


(b) Lift coefficient,(c_l) at different angles of attack, α

Figure 8. Lift and drag coefficient obtained on hydrofoil section at different angles of attack, α and *Re*s.



(a) Lift coefficient,(c_l) at different angles of attack, α_d



(b) Drag coefficient,(c_d) at different angles of attack, α_d

Figure 9. Lift and drag coefficient obtained on hydrofoil section at different duct angles, α_d and *Re*s.

at angle of attack, α = 0.15 ◦ respectively. It is noted that our results are in good agreement with the experimental results.

Figure 7 shows a negative pressure region on the upper surface of the hydrofoil, which extends from the leading edge till *x*/*c* = 0.5. At the trailing edge of the hydrofoil, vortices are seen to be generated leading to form a wake region.

Figure 8(a) shows the drag coefficient at a range of angles of attack, $-12^\circ \leq \alpha \leq 12^\circ$, while Figure 8(b) shows the lift coefficient in the same range of angles of attack. The results obtained are in strong accordance with experimental results of Hoffman[37]. The results in figures 8(a) and 8(b) shows that the grid metrics considered and the other values like fluid domain size and shape, mesh independency, aspect ratio, y+ value, orthogonality and grid skewness are considerably good for the present investigation. It is noted that departure from $\alpha = 0^\circ$ on either sides (+ve and −ve angles of attack), the drag force increases on the hydrofoil surface, However, in the range of $-4^\circ \leq \alpha \leq 4^\circ$, the increase in the drag values is insignificant.

The lift coefficient, c_l is seen to continuously increase with increasing α. At α =0˚, c_l is noted to be 0.3, which is noted to be 1.4 at α = 12˚. This suggests that till α =4˚, drag penalty will be minimal, while for higher angles of shroud angles (α_d), larger drag forces will act on the hydrofoil surface, affecting the overall efficiency.

4.2 Investigation of Effects of Shroud Configuration (Kort-nozzle duct) on Hydrodynamic Performance

In the following, an attempt is made to investigate analytical relationships for designing the Kort nozzle duct section using NACA-4415 hydrofoil. The preliminary stage was to develop the solution to a turbulent flow problem over a *2-D* configuration of a Kort-nozzle duct using NACA4415. The analysis was done for 0˚ ≤α ≤10˚ duct angle. A grid dependency study has been carried out with three combinations for better cell quality. The present results reported here are obtained with the best mesh from the generated ones. The overall lift and drag coefficients and the pressure distribution over the inside duct surface are studied here. The results are obtained both for steady and transient flow analysis. Figure 9(a) and (b) show the lift and drag coefficients (c_l and c_d) for values at 0˚ to 10˚ duct angle steady cases. The analysis is done for three sets of *Re* (1×10^6, 2×10^6, 5×10^6). With the increased duct angle, the pressure difference between the upper and lower surfaces increases, indicating the lift force increment in greater magnitude. But here, the axisymmetric configuration of the nozzle nearly nullifies the lift force effect.

The drag force acting on the hydrofoil operates in the direction of ship motion; hence it aids the thrust produced by the propeller. It is noted that the optimum angle of attack (shroud /duct angle, α_d) is between 3˚ to 4˚ for all the three *Re*s investigated. It is noted that the maximum drag is generated for lower *Re*. *Re* =1 $\times10^6$ and 5 $\times10^6$ at duct angle α_d =5˚ produce a considerably lower lift. However, for *Re* =2×10^6, we note a lesser lift at α_d =6˚. Considering various *Re*s at different shroud angles, it is

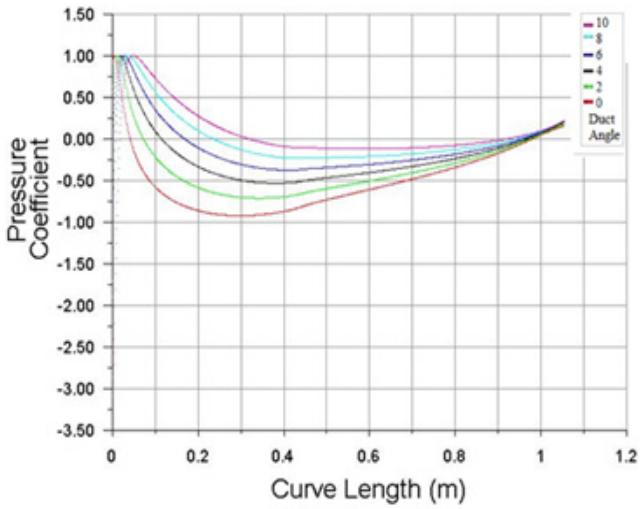
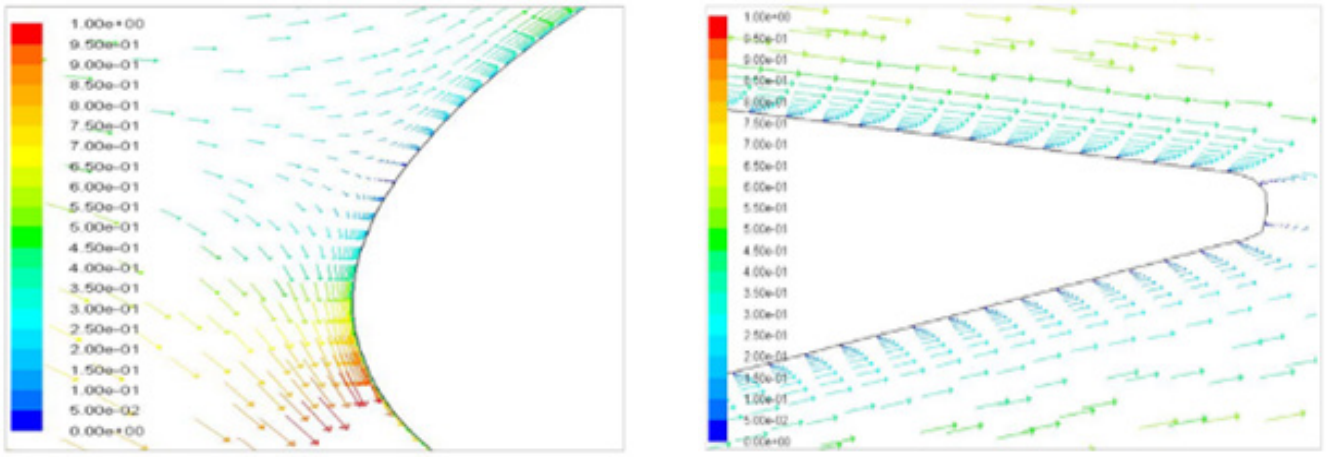


Figure 10. Pressure coefficient, c_p at different duct angles, α_d.



(a) Velocity vectors at the leading edge of the hydrofoil.

(b) Velocity vectors at the trailing edge of the hydrofoil.

Figure 11. Velocity distribution at the leading and the trailing edge of the hydrofoil, *Re* =2×10^5, α =4˚.

noted that the NACA4415 section exhibit better efficiency at a 3˚–4˚ duct angle.

The pressure distribution on the inner surface of the hydro-foil with respect to the duct angle, α_d is shown in Figure 10. At a α_d =4˚, the velocity vector plot, as shown in Figure 11. The velocity distribution near the leading edge and the trailing edge (see Figure 11(a) and (b)) shows attached flow, indicating no flow separation for this configuration. As seen from the figure, the max c_p values occur in the chord length $0.2 \leq x/c \leq 0.4$

5.0 Conclusions

The present study aims at understanding analytical relationships for designing the Kort nozzle duct section using NACA-4415 hydrofoil. The analysis was done for a range of duct angles. The objective was to establish the effect of duct angle on lift and drag coefficients. The standard CFD model and PISO algorithm were adopted for transient analysis. The velocity and pressure distribution, wall shear stress, and flow separation on the hydrofoil surface at different duct angles, along with the effect of increasing *Re*, were studied. The conclusions are as follows:

1) With the increased duct angle, the increase in drag coefficient is not noted up to α_d =4˚, but it shows a relatively higher magnitude at a duct angle of more than α_d =6˚. This indicates that a good range of duct angles can be set at α =3˚ to 4˚, for minimal drag penalty.

2) The wall shear stress increases with the increase of duct angle at the Leading Edge (LE), first increasing and then decreasing near the Trailing Edge (TE). At near *x/c* =0.7, the wall shear stress is the same for all duct angles.

3) With the increase of duct angle, the distribution of negative pressure on the duct's inner surface gradually moves from the head to the middle part of the hydro-foil. At α_d =4˚, this distribution gets uniform and lies approximately at the propeller plane, a favourable combination for higher thrust generation. This suggests that the position of the propeller should be within $0.2 \leq x/c \leq 0.4$ for optimum efficiency.

4) For the Kort nozzle, the NACA4415 hydrofoil section exhibit better efficiency with respect to thrust augmentation at a 3-4 degree duct angle for all range of *Re*s considered here.

6.0 References

1. Stipa L. Experiments with Intubed Propellers. L'Aerotechnica, Aug. 1931; pp. 923-53. Translated by Dwight M. Myner, NACA, NACA TM 655, Jan. 1932.
2. Stipa L. On the use of Propellers of Various Types, reprinted from L'Aerotechnica, March 1932; 8(3), translated by A. A. Fanelli for the Aerophysics department of Mississippi State College. 1956.
3. Kort, L. Der neue dusenschrauben-antrieb. Werft, Reederei und Hafen 1934; pp.15.
4. Carlton JS. Marine Propellers and Propulsion. Second Edition, Elsevier Publ., 2007. https://doi.org/10.1016/B978-075068150-6/50004-8
5. Tsakonas S, Jacobs, WR. Propeller Loading Distributions, Defense Technical Information Center, Accession Number: AD0682483, 1968. https://apps.dtic.mil/sti/citations/AD0682483
6. Fish Frank KE, Laurens EH, Mark MM, Hydrody-namic flow control in marine mammals. Integrative and Comparative Biology. 2008 Dec.; 48(6):788-800, https://doi.org/10.1093/icb/icn029 PMid:21669832
7. Fish Frank E, Hui Clifford A. Dolphin swimming-a review. Mammal Rev. 1991; 21(4):181-95. https://doi.org/10.1111/j.1365-2907.1991.tb00292.x
8. Gad-el-Hak M, Bushnell DM. Separation Control: Review. Journal of Fluids Engg.1991; 113:5-30. https://doi.org/10.1115/1.2926497
9. Schlichting H, Gersten K. Boundary Layer Theory. Springer Publ., 2017. https://doi.org/10.1007/978-3-662-52919-5
10. Viswanath PR. Some thoughts on separation control strategies. Sadhana. 2007; 32(1&2):83-92. https://doi.org/10.1007/s12046-007-0007-9
11. Taketani T, Kimura K, Ishii N, Matsuura M, Tamura T. Advanced Design of a ducted propeller with High Bollard Pull Performance. First International Symposium on Marine Propulsors SMP'09, Trondheim, Norway. June 2009.
12. Alejandro C, Marcos M, Adri'an S. CFD validation of different propeller ducts on open water condition. 13th Numer-ical Towing Tank Symposium; Duisburg Germany, Oct. 2010.

13. Celik F, Donguland A, Arikan Y. Investigation of optimum duct geometry for a passenger ferry. IX HSMV Naples. May 2011.
14. Long Yu, Greve M, Druckenbrod M, Abdel-Maksoud M. Numerical analysis of ducted propeller performance under open water test condition. Journal of Marine Science and Technology. 2013; 18(3):381-94.
15. Szafran K, Shcherbonos O, Ejmocki D. Effects of duct shape on ducted propeller thrust performance. Transactions of the Institute of Aviation; 2014; 237(4):84-91. https://doi.org/10.5604/05096669.1151026
16. He X, Zhao H, Chen X, Luo Z, Miao Y. Hydrodynamic Performance Analysis of the ducted propeller Based on the Combination of Multi-Block Hybrid Mesh and Reynolds Stress Model. Journal of Flow Control, Measurement and Visualization. 2015; 3:67-74. https://doi.org/10.4236/jfcmv.2015.32007
17. Chamanara M, Ghassemi H. Hydrodynamic characteristics of the Kort nozzle propeller by different turbulence models. American Journal of Mechanical Engineering. 2016; 4(5):169-72. https://doi.org/10.423610.12691/ajme-4-5-1.
18. Razaghian AH, Ghassemi H. Numerical analysis of the hydrodynamic performance of the accelerating and decelerating ducted propeller. Scientific Journals of the Maritime University of Szczecin. 2016; 47(119):42–53.
19. Majdfar S, Ghassemi H, Forouzan H. Hydrodynamic prediction of the ducted propeller by CFD solver. Journal of Marine Science and Technology. 2017; 25(3):268-75.
20. Majdfar S, Ghassemi H, Forouzan H. Hydrodynamic Effects of the length and angle of the ducted propeller. Journal of Ocean, Mechanical and Aerospace Science and Engineering. 2015; 25:19-25.
21. Majdfar S, Ghassemi H. Calculations of the hydrodynamic characteristics of a ducted propeller operating in oblique flow. Ship Science and Technology. 2017; 10(20):31-40. https://doi.org/10.25043/19098642.147
22. Moghaddam T, Neishabouri NB. On the Active and Passive Flow Separation Control Techniques over Airfoils. IOP Conference Series. Mater Sci Engg. 2017; 248:012009. https://doi.org/10.1088/1757-899X/248/1/012009
23. Eleni DC, Athanasios TI, Dionissios MP. Eval-uation of the turbulence models for the simulation of the flow over a National Advisory Committee for Aeronautics (NACA) 0012 airfoil. Journal of Mechanical Engineering Research. 2012; 4(3):100-11. https://doi.org/10.5897/JMER11.074
24. Seifert A, Pack LaTunia G. Oscillatory Excitation of Unsteady Compressible Flows over Airfoils at Flight Reynolds Numbers. 37th AIAA Aerospace Sciences Meeting and Exhibit, Reno, NV, 99-0925. 1999. https://doi.org/10.2514/6.1999-925
25. Sudarsono, Huda S, Rusianto T. Prediction of Aerodynamics Coefficients of Modified NACA 4415 Airfoil using Computational Fluid Dynamics. E3S Web of Conferences 202. 11002 ICENIS, 2020. https://doi.org/10.1051/e3sconf/202020211002
26. Oukassou K, El Mouhsine S, El Hajjaji A, Kharbouch B. Comparison of the power, lift and drag coefficients of a wind turbine blade from aerodynamics characteristics of NACA0012 and NACA2412. Procedia Manufacturing. 2019; 32:983-90. https://doi.org/10.1016/j.promfg.2019.02.312
27. Xu HY, Qiao CL, Yang HQ, Ye ZY. Delayed detached eddy simulation of the wind turbine airfoil S809 for angles of attack up to 90 degrees. Energy. 2017; 118:1090-109. https://doi.org/10.1016/j.energy.2016.10.131
28. Ke J, Edwards JR. Numerical Simulations of Turbulent Flow over Airfoils Near and During Static Stall. Journal of Aircraft. 2017; 54(5):1960-78. https://doi.org/10.2514/1.C034186
29. Baxevanou CA, Fidaros DK. Validation of Numerical Schemes and Turbulence Models Combinations for Transient Flow Around Airfoil. Engineering Applications of Computational Fluid Mechanics. 2008; 2(2):208–21 https://doi.org/10.1080/19942060.2008.11015222
30. Sarraf C, Djeridi H, Protein S, Billard JY. Thickness effect of NACA foils on global hydrodynamic parameters, boundary layer states and stall establishment. Journal of Fluids and Structures. 2010; 26(4):559-78. ISSN 0889-9746. https://doi.org/10.1016/j.jfluidstructs.2010.02.004
31. Bourgoyne DA, Hamel JM, Ciccio SL, Dowling DR. Time-averaged flow over a hydrofoil at high Reynolds number. J. Fluid Mech. 2003; 496:365-404. https://doi.org/10.1017/S0022112003006190

32. Shahsavarifard M. Effect of Shroud on the Performance of Horizontal Axis Hydrokinetic Turbines. Ph.D Thesis, University of Manitoba, Winnipeg. 2015 Mar. 96:215-25. https://doi.org/10.1016/j.oceaneng.2014.12.006
33. Breslin JP, Andersen P. Hydrodynamics of ship propellers. Cambridge Ocean Tech. Series, Cambridge Press, 1994. https://doi.org/10.1017/CBO9780511624254
34. Day AH, Babarit A, Fontaine A, He YP, Krakowski M, Murai M, Genesis I, Salvatore F, Shin K. Hydrodynamic modeling of marine renewable energy devices: A state-of-the-art review. Ocean Engineering. 2015; 108:46-69. https://doi.org/10.1016/j.oceaneng.2015.05.036
35. Bagade PM, Bhumkar YG, Sengupta TK. An improved orthogonal grid generation method for solving flows past highly cambered aerofoils with and without roughness elements. Computers and Fluids. 2014; 103:275-89. https://doi.org/10.1016/j.compfluid.2014.07.031
36. Samir BE, Mohammed A, Omar I, Fahri C. Effect of Geometric Configurations on Hydrodynamic Performance Assessment of A Marine Propeller. Brodogradnja/Shipbuilding. 2016; 67(4):31-48. https://doi.org/10.21278/brod67403
37. Hoffmann MJ, Ramsay RR, Gregorek GM. Effects of Grit Routghness and Pitch Oscillations on the NACA 4415 Airfoil. NREL/TP-442. 1996; 7815 https://doi.org/10.2172/266691